京都大学学術情報リポジトリ
KURENAI 紅
Kyoto University Research Information Repository

京都大学
KYOTO UNIVERSITY

Title	Thin layer composition profiling with angular resolved x-ray photoemission spectroscopy: Factors affecting quantitative results
Author(s)	Conard, T.; Vandervorst, W.; Bergmaier, A.; Kimura, K.
Citation	Journal of Vacuum Science & Technology A (2012), 30(3)
Issue Date	2012-04-20
URL	http://hdl.handle.net/2433/193695
Right	© 2012 American Vacuum Society
Type	Journal Article
Textversion	publisher

Kyoto University

Thin layer composition profiling with angular resolved x-ray photoemission spectroscopy: Factors affecting quantitative results

T. Conard, W. Vandervorst, A. Bergmaier, and K. Kimura

Citation: Journal of Vacuum Science & Technology A **30**, 031509 (2012); doi: 10.1116/1.4704603
View online: http://dx.doi.org/10.1116/1.4704603
View Table of Contents: http://scitation.aip.org/content/avs/journal/jvsta/30/3?ver=pdfcov
Published by the AVS: Science & Technology of Materials, Interfaces, and Processing

Articles you may be interested in
X-ray spectroscopic study of SrTiOx films with different interlayers
J. Appl. Phys. **113**, 224301 (2013); 10.1063/1.4809978

Beyond hard x-ray photoelectron spectroscopy: Simultaneous combination with x-ray diffraction
J. Vac. Sci. Technol. A **31**, 031103 (2013); 10.1116/1.4801915

Composition and structure of Pd nanoclusters in SiO x thin film
J. Appl. Phys. **109**, 084329 (2011); 10.1063/1.3561492

DepthResolved Composition and Chemistry of UltraThin Films by AngleResolved XRay Photoelectron Spectroscopy
AIP Conf. Proc. **788**, 307 (2005); 10.1063/1.2062980

In situ low-angle x-ray scattering study of phase separation in initially mixed Hf O 2 – Si O 2 thin film interfaces
Appl. Phys. Lett. **85**, 5884 (2004); 10.1063/1.1831554

AVS 61ST INTERNATIONAL SYMPOSIUM & EXHIBITION

Baltimore Convention Center

Redistribution subject to AVS license or copyright; see http://scitation.aip.org/termsconditions. Download to IP: 130.54.110.72 On: Mon, 08 Sep 2014 03:00:35

Thin layer composition profiling with angular resolved x-ray photoemission spectroscopy: Factors affecting quantitative results

T. Conard[a)]
IMEC, MCA, Kapeldreef 75, 3001 Leuven, Belgium

W. Vandervorst
IMEC, MCA, Kapeldreef 75, 3001 Leuven, Belgium and Instituut voor Kern-en Stralingsfysica, K. U. Leuven, Celestijnenlaan 200D, B-3001 Leuven, Belgium

A. Bergmaier
Institut f. Angewandte Physik und Messtechnik (LRT2) Fakultaet f. Luft- und Raumfahrttechnik Universitaet der Bundeswehr Muenchen Werner-Heisenberg-Weg 39, D-85577 Neubiberg, Germany

K. Kimura
Department of Micro Engineering, Kyoto University, Kyoto 606-8501, Japan

(Received 1 August 2011; accepted 31 March 2012; published 20 April 2012)

Composition profiling of thin films in the nanometer range is critical to the development of future electronic devices. However, the number of techniques with such depth resolution is limited. Among them, angle-resolved x-ray photoelectron spectroscopy (ARXPS) can be used for thin layers up to a few nanometers, but it is not yet a fully established method. In order to evaluate its capabilities for use as a routine and general method, the authors evaluate both its intrinsic capabilities in comparison with other methods and the factors affecting quantification by analyzing its variability when applied at various laboratory locations with different tools and data treatments. For this purpose, dedicated samples based on multilayers of HfO_2 and SiON were produced with a well-determined layer structure. The results show that ARXPS, including depth profiling reconstruction, is very efficient and compares favorably with nuclear analysis techniques. It allows the separation of the surface contamination signal from the interfacial layer signal and allows determination of the coverage quantitatively. An accuracy of ±10% is achieved for most elements except for nitrogen, where strong peak interference with hafnium and a low intensity increase the inaccuracy up to 20%. This study also highlights several technique limitations. First, the quality of the retrieved profile is strongly dependent upon the exact determination of each photoemission peak intensity. Also it demonstrates that, while favorable for chemical identification, very high resolution spectra may lead to larger errors in profile reconstruction due to larger statistical errors in the intensities, though this is true mainly for deeper layers. Finally, it points out the importance of the physical parameters used in the final obtained results. © *2012 American Vacuum Society*. [http://dx.doi.org/10.1116/1.4704603]

I. INTRODUCTION

In recent years the ongoing transistor performance increase has been possible thanks to, among other things, the introduction of materials with higher dielectric permittivity as a gate oxide.[1–3] As leakage current became unacceptable due to the decreasing gate oxide thickness, the replacement of SiO_2 by higher-k materials allowed for an increase of the physical thickness of the gate oxide (i.e., reduction of the leakage current) while keeping a low electrical thickness. The first devices based on this concept were made by introducing nitrogen into SiO_2.[4,5] Early on it was already recognized that the exact distribution of nitrogen in the gate oxide was a critical parameter in obtaining high performance.[4] However, the number of techniques with sufficient depth resolution to provide composition profiling within a few nanometers from the surface is limited. The most commonly known are transmission electron microscopy (TEM) combined with electron dispersive spectroscopy and/or electron energy loss spectroscopy (EELS)[6]; nuclear techniques such as high-resolution Rutherford backscattering spectrometry (HR-RBS),[7] medium energy ion scattering (MEIS),[8] or elastic recoil detection (ERD)[9]; time-of-flight (TOF-) secondary ion mass spectroscopy (SIMS)[10] and angle-resolved x-ray photoelectron spectroscopy (ARXPS).[11–13] In addition to accurate depth resolution and the possibility to quantify results, the best technique should be reasonably widespread and routinely available, which limits the use of nuclear analysis techniques. Although SIMS techniques have shown good nanometer scale profiling capabilities for SiON thin films,[14,15] it was also reported that most of the high-*k* profiles obtained by sputter depth profiling were plagued by ion beam sputtering artifacts.[16–19] Thus, a nonsputtering method like ARXPS, whereby the depth information is based on the depth dependent signal attenuation, may appear as a better candidate for thin film composition profiling. However, the latter requires a complex data reconstruction algorithm whose validity and uniqueness of results is still debated[13] and where the potential method limitations even for simple systems such as SiON (Ref. 20) have been indicated.

Notwithstanding these considerations, ARXPS reconstructed depth profiles have already been applied to many different

[a)]Electronic mail: thierry.conard@imec.be

Redistribution subject to AVS license or copyright; see http://scitation.aip.org/termsconditions. Download to IP: 130.54.110.72 On: Mon, 08 Sep 2014 03:00:35

systems with various successes.[21] Given the limitation of sputtering techniques for high-k materials, it appeared necessary to study ARXPS possibilities and limitations in more detail. In order to consider its capabilities as a routine and widespread method, we approached this assessment not only by analyzing the intrinsic capabilities of the method in comparison to other analysis methods, but also by analyzing its variability when applied at various laboratory locations. For this purpose, dedicated multilayer samples of HfO_2 and SiON were produced with a well-determined layer structure and analyzed through different techniques. Rather than imposing a standard analysis method/protocol (which was not possible due to tool and software diversity), each participant was free to use his own "optimum" approach. With this motivation, one can capture the errors currently occurring across the entire community when similar structures are (routinely) analyzed. Based on this study, the need for a stricter protocol and a more consistent data treatment can be identified.

II. EXPERIMENT

A. Sample description

Each sample was formed by growing a dedicated stack on 200 mm Si wafers, as described in Table I. Layer thicknesses given in Table I are only indications, as they correspond to the nominal/processing thicknesses. The production processes selected to produce the different layers were such that sharp interfaces are expected between each layer.

As the high-*k* layer, we selected a 2.5 nm HfO_2 layer grown by atomic layer deposition (ALD) at 300 °C from $HfCl_4$ and H_2O precursors. This process was selected due to its good uniformity and its low growth temperature, thereby avoiding potential indiffusion or intermixing. As this ALD process does not produce high quality layers when grown directly on Si,[22,23] an interfacial layer was introduced. We selected either a 1 nm chemical oxide, grown by an ozonated process (IMEC clean),[24] or a 1.6 nm SiON layer produced by a direct plasma nitridation process.[25]

On top of the HfO_2 layer, a third layer was grown for samples 1, 4, and 5. This third layer was an Si_3N_4 CVD layer that was expected to oxidize in the air. The thickness of the top Si_3N_4 layer was chosen to be ~2 nm for sample 1 and ~0.5 nm for samples 4 and 5.

On sample 1, both a thicker HfO_2 (5 nm) and a thicker SiON (2 nm) layer were produced in order to test the possibility of distinguishing an SiO_2 layer under a thick layer while an Si(O)N layer is present at the top surface. Hence, such a thick layer structure is expected to be beyond the XPS capabilities. Samples 2 and 3 were designed as simple two-layer systems with or without nitrogen at the bottom interface, while samples 4 and 5 were complicated by the presence of nitrogen and Si also present at the top surface.

TABLE I. Sample description.

Sample number	Top	High-k	Interface	Substrate
1	SiON 2 nm	HfO_2 5.0 nm	SiO_2 1 nm	Si
2		HfO_2 2.5 nm	SiO_2 1 nm	Si
3		HfO_2 2.5 nm	SiON 1.6 nm	Si
4	SiON 0.5 nm	HfO_2 2.5 nm	SiO_2 1 nm	Si
5	SiON 0.5 nm	HfO_2 2.5 nm	SiON 1.4 nm	Si

The choice of HfO_2 as the high-k material resulted from its industrial relevance. It must be mentioned that, in this case, additional difficulties arose for XPS to retrieve the nitrogen concentration. Indeed, there is interference between the N 1*s* photoemission peak and the energy loss peak from the Hf4*d* photoemission peak leading to difficult nitrogen quantification at low concentration in Hf-based materials.

B. Sample qualification

1. Uniformity

In order to perform a reliable results comparison between the different measurement approaches, we must ensure that all the measurements are performed on an identical sample structure, which, of course, raises the question of the production process uniformity. All samples corresponding to the same layer structure originated from the center part (~12×12 cm^2) of a single wafer. The uniformity investigation was performed in two successive steps. First, ellipsometry measurements were performed using an F5 spectrometer from KLA-Tencor. The thickness measurements were analyzed using a single-layer model. As a consequence, the measured thickness should not be taken as absolute exact values, but only as indications of relative variations.

Figure 1 presents the thickness and standard deviation measured on samples 2–5. The standard deviation across the wafer was measured in a circular mapping of 81 points with a 10 mm exclusion edge and, in all cases, was found to be less than 0.1 nm, which highlights the reproducibility of the measurements. Although the measured thicknesses should not be taken as absolute exact values, they do reflect the expected variations in relation to differences in process conditions.

Regarding the across-wafer uniformity, a thickness gradient was observed on all wafers (Fig. 2). In order to identify the origin of the measured gradient, ARXPS mapping was

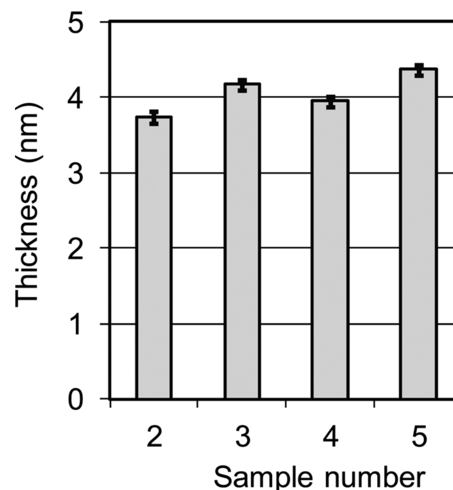

FIG. 1. Average ellipsometry thickness (nm) and their standard deviation measured on 81 points at the wafer surface.

Redistribution subject to AVS license or copyright; see http://scitation.aip.org/termsconditions. Download to IP: 130.54.110.72 On: Mon, 08 Sep 2014 03:00:35

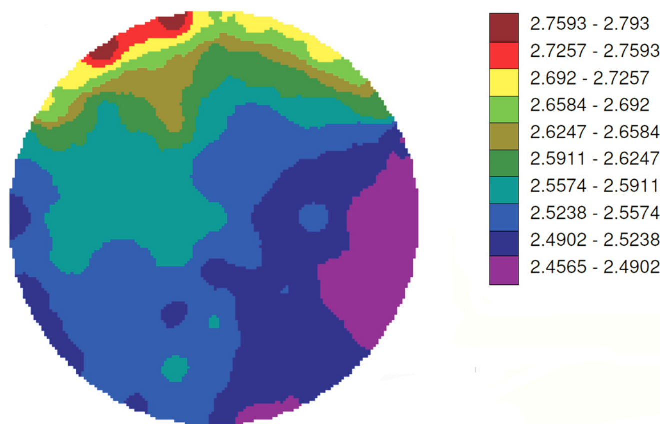

FIG. 2. (Color online) Ellipsometry thickness mapping (nm) of sample 5.

performed on all samples (data not shown). According to these data, it is clear that the gradient originated from a slightly thicker HfO_2 layer at the edge of the wafer. The HfO_2 thickness variation remains limited to a maximum of 1 Å within the limited 12×12 cm^2 area used for this study, which was not considered to be critical for the study (Table II).

2. Sample stability

Since samples were measured over an extended period of time, their stability should be checked. Particularly for the three samples with a surface Si_3N_4 layer it was important to analyze the aging (oxidation) of this layer as a source of discrepancy between the different groups. In order to analyze this effect, we measured the XPS spectra soon after the layer deposition and again several months later. The results are presented in Fig. 3. On the Si 2*p* spectra from sample 1, a clear increase in intensity on the high binding energy side is observed with aging, due to surface oxidation of the Si_3N_4 layer. The measured top oxide thickness grows from ~0.4 nm shortly after deposition to ~1.1 nm, typical of a native oxide after several months of air exposure. In sample 4, one sees an important decrease (~1/3) in the measured nitrogen dose after aging. This, unfortunately, leads to a nitrogen concentration at the surface below the detection limit for HR-RBS. All results presented in this work relate to measurements performed on aged samples, which can be considered as fully stabilized and suited for intercomparison.

TABLE II. Average HfO_2 and SiO_2 thickness, standard deviation, and absolute thickness range measured on the 120 central millimeters of each wafer.

Wafer	Material	Mean (nm)	Sigma (%)	Range (abs) (nm)
1	HfO_2	3.27	2.60	0.35
	SiO_2	1.40	1.23	0.08
2	HfO_2	2.12	1.15	0.11
	SiO_2	0.81	6.56	0.23
3	HfO_2	2.21	0.99	0.09
	SiO_2	1.37	3.33	0.16
4	HfO_2	2.32	1.22	0.13
	SiO_2	1.05	1.02	0.04
5	HfO_2	2.54	1.30	0.14
	SiO_2	1.21	0.91	0.05

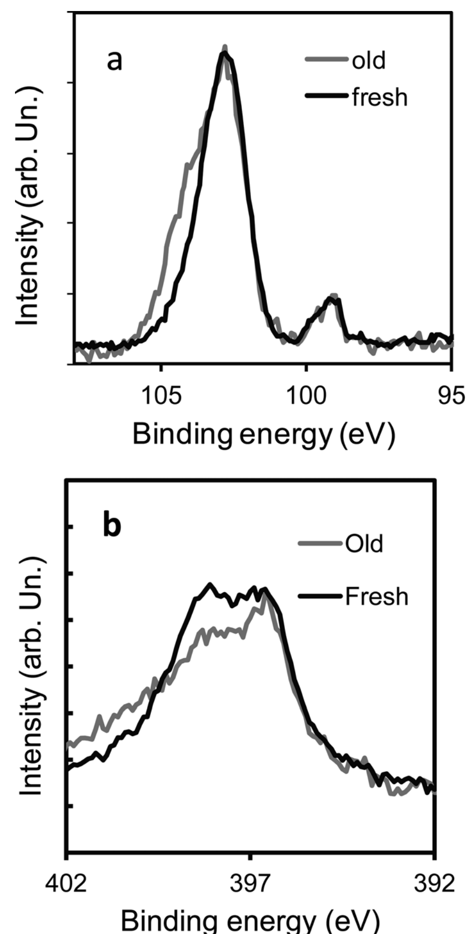

FIG. 3. Si 2*p* spectra (a) from sample 1 and N 1*s* spectra (b) from sample 4 measured soon after processing (black) and after several months (gray).

C. Analysis techniques

This work deals with the results from 12 groups and covers several techniques. The techniques used in this study are based on electron microscopy: TEM (two groups); ion beam analysis: HR-RBS (two groups); ERD (one group); MEIS (one group) and XPS. Distinction should be made between ARXPS by sample tilting (three groups) and ARXPS in parallel acquisition mode (four groups). Throughout this article, the results will be identified by their group number as given in Table III. Not all groups have reported results for all samples. In addition, composition depth profiles were not reported by the "tilted ARXPS" groups.

TEM experimental details were the following: for one group, samples were analyzed by means of cross-section transmission electron microscopy. The TEM was used in scanning mode with an electron beam diameter of <0.3 nm. Imaging was done using a so-called HAADF detector, giving predominantly Z-contrast images (heavy elements appear bright). Elemental composition was studied by means of EELS and energy dispersive x-ray analysis. The other group used a Tecnai F30 operating at 300 kV with an electron-beam diameter of ~1 nm. The sample preparation method was conventional ion milling (precision ion polishing system).

MEIS analyses were carried out using a nominally 100 keV He^+ ion beam in double alignment configuration,

Redistribution subject to AVS license or copyright; see http://scitation.aip.org/termsconditions. Download to IP: 130.54.110.72 On: Mon, 08 Sep 2014 03:00:35

TABLE III. List of groups involved in the intercomparison together with the technique applied.

Group number	Technique
1	ARXPS (AR nontilted sample mode)
2	HR-RBS
3	TEM
4	TEM
5	MEIS
7	ARXPS (AR nontilted sample mode)
9	ARXPS (AR nontilted sample mode)
10	ERD
12	ARXPS (AR nontilted sample mode)
13	XRR
4	XPS (AR tilted mode)
15	XPS (AR tilted mode)
16	HR-RBS

where the channeling direction was along the [−1−11] axis and the blocking direction along the[111] axis. The overall near-surface depth resolution obtained for these conditions was better than 0.7 nm, with the resolution reducing with increasing depth in the sample due to energy straggling.

The HR-RBS measurements were performed using an analysis beam of 450 keV He^+ at an incident angle of 45° from the normal to the ⟨101⟩ plane of the sample.

High resolution elastic recoil detection measurements were performed on a 14 MV tandem accelerator. A 40 MeV Au ion beam at an incident angle of 10° with respect to the surface plane was used. Such a heavy incident ion can recoil target atoms in the forward direction and these recoiled ions were momentum analyzed by a Q3D magnetic spectrograph and detected by a gas ionization chamber. The energy resolution of the spectrograph was 0.05% with an acceptance angle of 5 mrad. This excellent energy resolution ensures a depth resolution better than 1 nm at the surface. The Si profile from sample 3 was also measured with 170 MeV iodine ions.

The ARXPS measured in tilted mode were performed on three different instruments. All used monochromatized Al $K\alpha$ radiation. The spectrometers were operated with a wide angular acceptance of 30°–40° and cannot be considered as high-resolution ARXPS.

All ARXPS in the parallel detection mode experiment were performed on Theta instruments from ThermoInstrument, using monochromated Al $K\alpha$ radiation at 16 different emission angles between 22° and 78° as measured from the normal of the samples. Different energy resolutions were used for the measurements performed by different groups.

III. RESULTS AND DISCUSSION

A. Methodology

1. Studied layer characteristics

Three main characteristics were compared on the different samples: thickness, composition profile, and chemical state. This study will focus on the analysis of layer thickness and composition profile since XPS is the only technique able to provide information about chemical states.

Regarding thickness, both individual layer thickness and total layer thickness will be compared. Indeed, a larger error/discrepancy is expected for the individual thickness. Individual layer thickness may also not be available in all cases, particularly when only composition profiles are retrieved from the data. In the THERMO software, the mean free paths derived from the TPP-2 model were selected.[26] It was checked that these mean free paths corresponded to the National Institute of Standards and Technology (NIST) effective attenuation length database (within 2%).[27]

Also, full depth profiles could not always be directly compared from one group to another. First, due to the difference in analysis technique, one does not obtain comparable information; for instance, XPS profiles can be decomposed into profiles from different chemical states, while TEM, HR-RBS, MEIS, and ERD only have access to elemental information. Thus, depth profile will be compared mainly from an elemental composition profile point of view. The XPS data were converted by adding together all concentrations from a given element. Second, errors in total thickness appeared due to inaccuracies in the parameters (mean free path length, stopping power, material density, etc.) determining the depth scale. For nuclear techniques and photoemission we have to assume material densities in order to reconstruct the profiles. The densities used in this study were taken from Ref. 28. Finally, uncertainties in emission angles, scattering angles, etc., may introduce additional errors propagating through the entire depth profile. Hence a direct comparison (without any normalization) reveals strong differences. In order to understand their origin (data algorithm, resolution, calibration, etc.), a further comparison is performed in two steps. First, a qualitative comparison of the profile shape is performed by rescaling the profile in order to align the interface with the Si substrate. This removes all uncertainties on depth scale and allows us to understand the factor limiting depth sensitivity and concentration quantification. In a second step, a quantitative comparison is performed based on calculated atomic coverages (doses in at./cm^2).

2. XPS data treatment

a. Nitrogen interference. One of the major issues for XPS data treatment is the determination of the nitrogen intensities and, thus, N concentrations. As mentioned earlier, strong intensity interference occurs between the N 1*s* peak and the energy loss peak of the Hf4*d* peak. Different groups did use different methods to remove this interference, as listed in Table IV, which leads to major differences between nitrogen concentration determinations. For instance, on sample 3, group 12 reported the absence of nitrogen. This evidenced the first (expected) critical factor in the use of ARXPS: standardized background estimation is crucial for obtaining systematic results. As a consequence, a unified data treatment was applied to all ARXPS data: N 1*s* intensities were retrieved by fitting the N 1*s* region with an

Redistribution subject to AVS license or copyright; see http://scitation.aip.org/termsconditions. Download to IP: 130.54.110.72 On: Mon, 08 Sep 2014 03:00:35

TABLE IV. Data treatment summary from participating XPS groups.

Group 1:	Si 2*p*: A single peak was used for the oxidized and nitrided Si component, except for sample 1, where two peaks were used.
	O 1*s*: Total O intensity was used.
	N 1*s*: The experimental spectrum from an HfO_2 film was used as background and a nitrogen peak was added for the fit.
	THERMO software was used for depth profile reconstruction.
Group 7:	Si 2*p*: Two peaks were used for the oxidized and nitrided Si component.
	O 1*s*: Two peaks were used corresponding to oxygen bounded to Hf and to Si, respectively.
	N 1*s*: A single peak (FWHM limited) was used on top of a Shirley background.
	THERMO software was used for depth profile reconstruction.
Group 9:	Si 2*p*: A single peak was used for the oxidized and nitrided Si component, except for sample 1, where two peaks were used.
	O 1*s*: Total O intensity was used.
	N 1*s*: The plasmon peak from Hf was fitted with Gaussian–Lorentzian peaks and N 1*s* peaks were added.
	THERMO software was used for depth profile reconstruction.
Group 14:	Total peak intensities were used for compositional profiling.
	Depth profiles were calculated from a maximum entropy method but were used mainly to determine the "layering" of the system.
	N 1*s* peak was fitted with a linear background and several chemical states.
Group 15:	Hf, Si, and O peaks were fitted using multiple chemical components.
	Total intensity of N 1*s* above a linear background was used.
	ARCTICK software was used for layer thickness and stratification.
	This group was the only one using the Hf4*d* peaks for Hf analysis; the other groups were using the Hf4*f* peak.

experimental loss spectrum of the Hf4*d* peak and a Gaussian–Lorentzian component.

b. Layer thickness determination. In TEM, thickness extraction is a direct measurement of the recorded images. For nuclear techniques, thicknesses are derived from the conversion of the atomic coverage (at./cm^2) using standard densities.[28] In XPS, layer thickness calculations were performed using the model described in Ref. 29. For a thin layer on a substrate, the equation providing the thickness is given by

$$d = \lambda \cos(\theta) \ln\left[1 + \frac{R}{R_0}\right],$$

where d is the layer thickness, λ is the mean free path of the detected electron in the overlayer, θ is the angle of emission, R is the intensity ratio of the overlayer on the substrate, and R_0 is the intensity ratio of a semi-infinite layer of the considered elements.

This model can be generalized for multiple layers with a sharp interface by fitting the angular dependence of the intensity ratio between adjacent layers.[29] One severe limitation of this method is that each layer has to be represented by an independent photoemission peak. For instance, in this study the layer thickness of the triple stack SiON/HfO_2/SiON cannot be determined because the same elements are present in the top and the bottom layer.

c. Depth profile reconstruction. The depth profile reconstruction from ARXPS data was performed using a maximum entropy routine similar to the one described in Ref. 30. It is well known that no unique solution is achieved in the conversion of ARXPS intensities into composition depth profiles, which makes least square fitting unfeasible. The introduction of the entropy term allows stabilizing the solution and the optimization is achieved by maximizing the join probability function,

$$Q = \alpha S - 0.5\chi^2,$$

where the entropy term is given by

$$S = \sum_j \sum_i c_{j,i} - c^0_{j,i} - c_{j,i} \log\left(\frac{c_{j,i}}{c^0_{j,i}}\right),$$

with $c_{j,i}$ representing the concentration of element i in layer j and α is a regularizing parameter.

The profiles were reconstructed using the ThermoInstrument software ARPROCESS. In this reconstruction, the mean free path is determined using a two-layer model (HfO_2/Si) with the TPP2 formula, i.e., using a unique mean free path per photoemission peak through the whole overlayer. Stoichiometric constraints are used in the overlayer. This procedure leads to realistic depth profiles reflecting the overall shape, but they are susceptible to deviations regarding depth scale as a consequence of the assumption of a homogeneous overlayer for the mean free path. When incorrect depth scales are used with assumed bulk densities errors will be propagated to the conversion into element coverage. This software also does not take into account possible elastic scattering effects. A more physically based approach is possible using Simulation of Electron Spectra for Surface Analysis (SESSA) software from NIST-TU Wien.[31,32] Auger-electron and photoelectron spectra can be simulated for layered samples based on physical parameters present in several databases; differential inverse inelastic mean free paths, total inelastic mean free paths, differential elastic scattering cross sections, total elastic scattering cross sections, transport cross sections, photoelectric cross sections, photoelectric

Redistribution subject to AVS license or copyright; see http://scitation.aip.org/termsconditions. Download to IP: 130.54.110.72 On: Mon, 08 Sep 2014 03:00:35

asymmetry parameters, electron-impact ionization cross sections, photoelectron line shapes, Auger-electron line shapes, fluorescence yields, and Auger-electron backscattering factors. The simulated spectra, created using layer compositions and thicknesses specified by the user, can be compared with measured spectra and layer compositions and thicknesses can then be adjusted to find the maximum consistency between simulated and measured spectra. In this work, XPS data were simulated using internal databases provided with the software. The sample models were based on a multilayer structure reflecting the processing sequence (two or three homogeneous layers), with an additional "surface contamination" layer containing C and O. The structures are simulated with a sharp interface as expected from the processing parameters. For each layer, thickness and composition were modified in order to achieve a satisfactory agreement between the measured and calculated angular dependent XPS intensities. However, as no optimization routine is provided, SESSA is not suited for full depth profile reconstruction and was only used as a check for quantitative profiles.

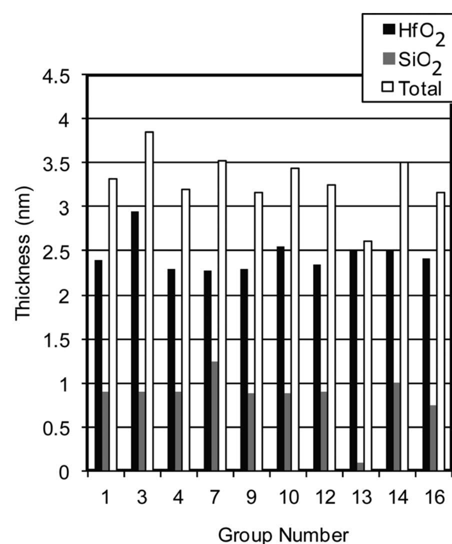

FIG. 4. Layer thickness (nm) determined for sample 2 by each of the groups. The total thickness is the sum of the SiO_2 interfacial layer thickness and the HfO_2 layer thickness.

B. Reference profile

For each of the studied samples reference profiles were needed to evaluate the accuracy of the ARXPS profiles. For that purpose, nuclear techniques were included as they should provide an accurate reference profile. According to Amsel and Battistig, [33]"While Ion Beam Analysis (IBA) is insensitive to the chemical state of the atoms analyzed, it is unique in particular for determining with high accuracy and sensitivity absolute atomic quantities or concentrations […]." Unfortunately, for the structures studied in this project that assumption is far from reality. Indeed, even for the simplest layer structure (sample 3: HfO_2/SiON/Si) significant discrepancies were observed between the three nuclear techniques. Even qualitatively, substantial differences between these methods have been observed.[7,11,34,35] For instance, profiles recorded from ERD measurements with 40 MeV Au show a significant amount of Si inside the HfO_2 layer. This is clearly an artifact created by strong multiple scattering; it is easy to prove by techniques such as TOF-SIMS that there is not any Si in the layer. As an alternative, sample 3 was also measured with ERD using 170 MeV iodine, which removes the artifact. In this case, a good agreement is obtained between ERD and HR-RBS. However, as HR-RBS also suffers from a relative lack of sensitivity to nitrogen, in particular for the capped layers, the ERD profiles will be used in the rest of this article as reference profiles where no nitrogen is detected by HR-RBS. However, since not all samples were remeasured by ERD the ERD Si intensity in the HfO_2 layer will be neglected.

C. Physical information

1. Layer thickness

a. HfO_2/SiO_2/Si (sample 2). The simplest sample of this study has a double-layer structure HfO_2/SiO_2/Si (sample 2). Figure 4 presents the thickness determined by the different groups with the different analysis techniques. It presents both the individual layer thickness of the HfO_2 and SiO_2 layer as well as the total layer thickness. The determination of the SiO_2 layer thickness is fairly reproducible between the different techniques. Taking all data into account, we find the HfO_2, SiO_2, and total layer thickness to be on average 2.46, 0.85, and 3.30 nm with a standard deviation of 0.20, 0.29, and 0.32 nm, respectively. Clear outliers are found for group 7 (ARXPS) and group 13 [X-ray reflectometry (XRR)] on the SiO_2 layer thickness. Group 16 (HR-RBS) is not considered as an outlier because the thickness has been calculated from the oxygen depth profile with a very low data density, leading to a substantial uncertainty. The very small SiO_2 thickness determined by XRR is a consequence of the difficulty to determine the interface thickness due to the small difference in electronic density between SiO_2 and Si. The large SiO_2 interfacial layer observed by group 7 can be explained by a contamination problem (which is described in more detail later). The HfO_2 layer thickness presents only one outlier for group 3, which is not explained. If the understood outliers for the SiO_2 layer thickness are not taken into account, the average thickness increases slightly to 0.89 nm, but the standard deviation drastically decreases to 0.07 nm.

Concentrating on the ARXPS data, Table V presents the layer thickness of each layer of sample 2 in a three-layer model (see Sec. III A 1), including a carbon surface

TABLE V. Thickness (nm) of each layer of sample 2 as determined by the four groups using parallel angle-resolved XPS.

Group	C	HfO_2	SiO_2	Total
1	0.20	2.4	0.91	3.31
7	0.61	2.28	1.25	3.53
9	0.40	2.29	0.88	3.17
12	0.22	2.35	0.91	3.26

Redistribution subject to AVS license or copyright; see http://scitation.aip.org/termsconditions. Download to IP: 130.54.110.72 On: Mon, 08 Sep 2014 03:00:35

contamination layer. Table V shows that a very good repeatability of the determined thickness is obtained, which is also close to the average value measured by the different techniques independent of the contamination layer thickness. As noticed previously, the interfacial layer thickness of group 7 appears much thicker than in the other groups. In fact, a more detailed analysis from the ARXPS data shows that the contamination layer also contains some Si, as in the three-layer model, although Si is assumed to be present only at the interface. Of course, this additional surface intensity translates into a larger apparent thickness. Obviously, model-based quantification requires a correct model and the advantage of angle-resolved XPS compared to single-angle XPS clearly appears here. While, in single-angle XPS, the model used to retrieve thickness can only be based on processing sequences, the larger data set available in an ARXPS experiment allows for improvement of the model definition. Neglecting the outlier, the agreement is also remarkable because it is obtained for data recorded in a wide range of measurement conditions. Indeed, analyzer pass energies vary from 30 to 200 eV and the angular range used for the calculation also slightly varies between the instruments (ThetaProbe versus Theta300). These layer thicknesses are also in very good agreement with the thicknesses determined by nuclear techniques (ERD and HR-RBS) when identical densities are assumed for all techniques.

b. HfO_2/SiON sample (sample 3). Figure 5 presents the layer thickness determined by each group for the HfO_2/SiON double stack. The agreement between the XPS thickness (groups 1, 7, 9, 12, and 14) and the nuclear techniques thickness (groups 2, 10, and 16) for the HfO_2 thickness is very good (average of 2.3 nm $\pm$ 0.1 nm compared to an average of 2.44 nm $\pm$ 0.1 nm). The agreement for the interfacial layer thickness is poorer, mostly for HR-RBS. The interfacial layer thickness is indeed much more difficult to determine by this technique due to a lower sensitivity to nitrogen and to the low data density in the profile which leads to larger errors. The agreement for the interfacial layer thickness between ARXPS and ERD is better (1.6 $\pm$ 0.2 nm vs 1.4 nm). To obtain the interfacial layer thickness by ERD, the amount of excess oxygen at the interface is calculated assuming a stoichiometric HfO_2 layer and was converted to an SiO_2 layer thickness assuming stoichiometric SiO_2. Similarly, a layer thickness of Si_3N_4 was calculated based on the nitrogen dose measured at the interface. The total interfacial layer thickness is the sum of the calculated SiO_2 and Si_3N_4 thicknesses. Similar to that observed for the HfO_2/SiO_2 sample, larger differences are seen with TEM and XRR data.

c. SiON/HfO_2/SiO_2 and SiON/HfO_2/SiON (samples 4 and 5). As mentioned earlier, the layer model is not applicable for these samples as it requires a unique photoemission peak in each layer.

2. Composition profile

a. HfO_2/SiO_2/Si sample (2). Figure 6 presents the composition profiles reconstructed from sample 2 by groups 1 and 7 using ARXPS in parallel mode. The profiles were reconstructed as a mixture of stoichiometric HfO_2 and SiO_2 units, allowing for excess C and O to be accounted for as possible surface contamination. As the carbon contamination layer thickness is much larger for the measurements from group 7, depth scales were shifted by the thickness of the C contamination layer. In this case, an excellent agreement of the two profiles is obtained, including the interfacial layer thickness. This comparison explains the apparent larger SiO_2 interfacial layer thickness obtained by group 7 when using only intensity ratios. Indeed, the profile from group 7 shows a slight increase of Si intensity toward the sample surface. Combined with the much larger C contamination layer thickness observed, this shows that the surface contamination also includes some silicon, possibly in the form of silicon oils.

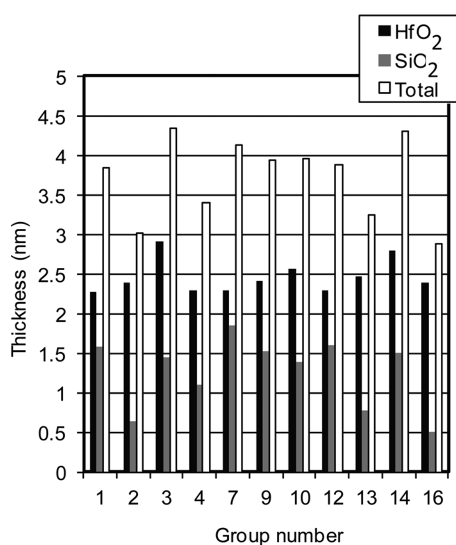

Fig. 5. Layer thickness (nm) determined for sample 3 by each of the groups. The total thickness is the sum of the SiO_2 interfacial layer thickness and the HfO_2 layer thickness.

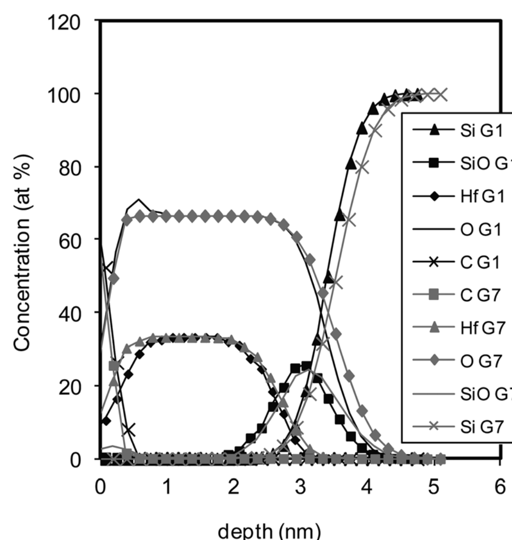

Fig. 6. Comparison of reconstructed composition profiles from ARXPS data for sample 2 from group 1 (G1) and group 7 (G7).

Redistribution subject to AVS license or copyright; see http://scitation.aip.org/termsconditions. Download to IP: 130.54.110.72 On: Mon, 08 Sep 2014 03:00:35

The repeatability of the profile obtained by ARXPS does not yet imply that the results are accurate. In order to verify this aspect, the profiles were compared to the profiles obtained by ERD (Fig. 7). To make comparison easier, intensities corresponding to the SiO_2 interface and Si substrate were added into the XPS profile since there is not any chemical information in the ERD profile. A significant difference is seen, mostly at the interface where the XPS profile has an apparent sharper profile. This is mostly due to the degraded depth resolution of the ERD with increased depth. It should be mentioned, however, that the XPS profile reconstruction algorithm imposes a 100% Si concentration in the substrate and thus "sharpens" the interface. The depth scale of the ERD profile was converted from the standard at./cm^2 to nm using densities of the HfO_2, SiO_2, and Si, respectively. In this way a good agreement is obtained between the XPS and ERD profiles.

b. HfO_2/SiON sample (sample 3). The profile reconstructed from the ARXPS data on sample 3 is close to the expected one and is in reasonably good agreement with the ERD profile (Fig. 8), except for a lower N concentration at the interface in the ERD profile. Contrary to the other ERD profiles, these measurements have been performed with 170 MeV I particles instead of 40 MeV Au ions. This has the following advantages: The reduction of the strong multiple scattering, which leads to an improvement of depth resolution and the reduction of the unrealistic Si profile inside the HfO_2 layer.

c. SiON/HfO_2/SiON (sample 5). For XPS, the SiON/HfO_2/SiON triple-layer sample is particularly challenging because the same elements (Si, O, N) are present both in the top layer and in the interfacial layer. It also renders the simple model for layer thickness calculation based on pure intensity ratios inefficient, since unique photoemission peaks cannot be found in each layer independently. We thus have to rely on full profiling only.

Figure 9 presents composition profiles obtained from angle-resolved data by four different groups. A very good agreement is obtained by three of the groups, while the fourth group's profile shows the HfO_2 layer extending deeper with a thinner interfacial layer. This last profile originates from the data recorded with the lowest analyzer pass energy, i.e., with the highest statistical noise. This leads to

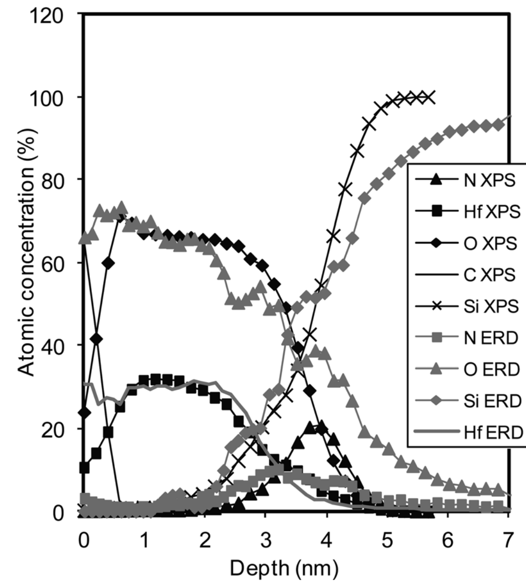

Fig. 8. Comparison of reconstructed composition profiles from angle-resolved x-ray photoelectron spectroscopy (ARXPS) data for sample 3 from group 1 and the elastic recoil detection (ERD) profile.

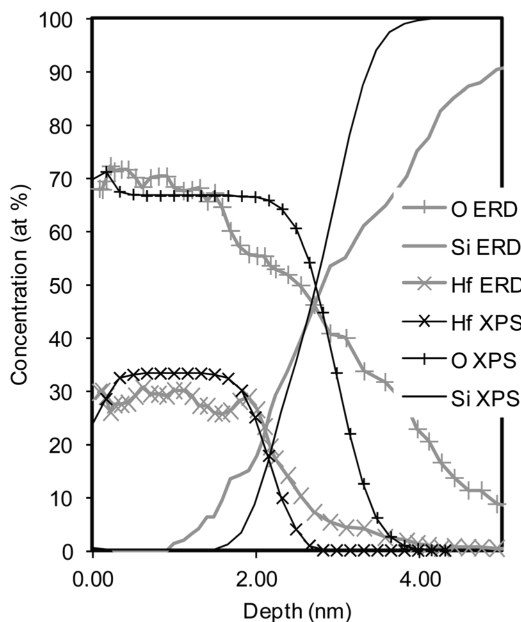

Fig. 7. Comparison of reconstructed composition profiles from angle-resolved x-ray photoelectron spectroscopy (ARXPS) data for sample 2 from group 1 and the elastic recoil detection (ERD) profile.

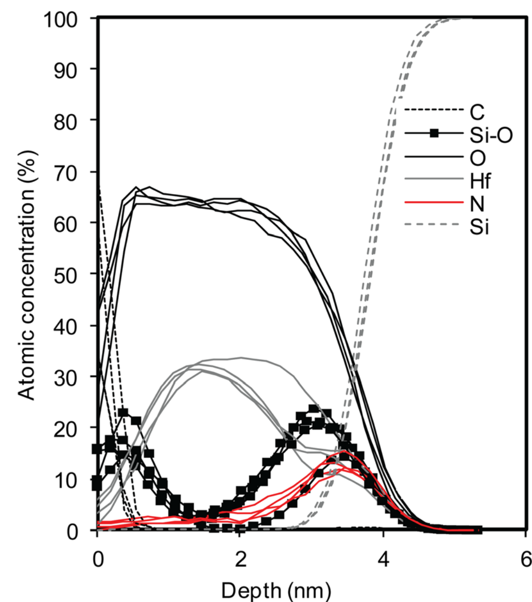

Fig. 9. (Color online) Comparison of the atomic concentration depth profiles obtained by four different groups after applying an identical data treatment procedure on wafer 5. The silicon concentration has been split into two different chemical contributions: elemental silicon (Si) and bounded silicon (Si–O).

Redistribution subject to AVS license or copyright; see http://scitation.aip.org/termsconditions. Download to IP: 130.54.110.72 On: Mon, 08 Sep 2014 03:00:35

the third critical parameter for profile reconstruction: statistical noise should be reduced as much as possible for a reliable depth profile reconstruction. The impact of statistical noise is also enhanced by the fact that the total layer thickness is, according to the process condition, close to 4.6 nm, which approximates the limit to which reliable profiles can be extracted. On these profiles one can observe that, while the reacted (to O or N)–Si composition profile is clearly identified in two separate layers at the surface and at the interface, the nitrogen profile does not present a surface peak as would be expected. However, it is also clear that, compared to the nitrogen profile obtained for the double-layer stack [HfO_2/SiON/Si (Fig. 8)], the nitrogen extends closer to the surface. The differences between the reacted-Si and nitrogen profiles are likely due to a still imperfect spectrum deconvolution of the N 1*s* photoemission peak.

Figure 10 presents the comparison of the N and Si profiles obtained by XPS and ERD. In order to determine the profile of reacted Si at the interface in ERD, the excess oxygen in the profile compared to HfO_2 was converted to an Si profile, assuming an SiO_2 layer, and the nitrogen profile at the interface was converted to an equivalent Si profile, assuming Si_3N_4. The agreement both at the interface and at the surface is, in this case, very good for the Si profile. Inside the HfO_2 layer, the Si profile is known to be less reliable by ERD due to the strong multiple scattering in the measurement conditions (40 MeV Au). An improved Si profile in the HfO_2 layer, which can be obtained by using higher energy particles, is not available for this sample. The nitrogen profile from XPS at the interface also compares favorably with the ERD profile but, as mentioned earlier, the XPS does not correctly reproduce the ERD nitrogen profile at the surface.

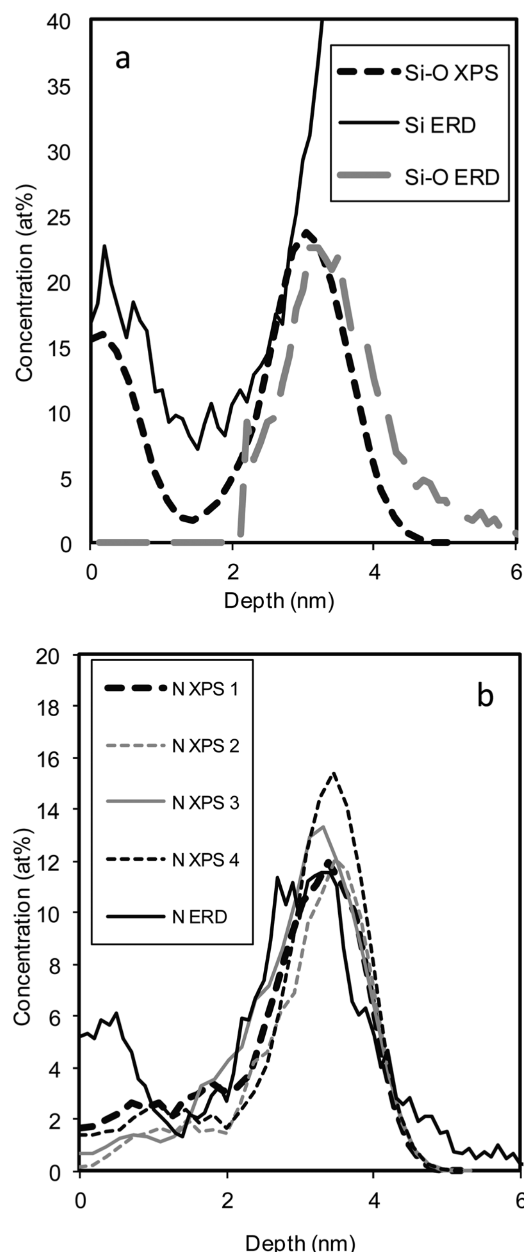

FIG. 10. Comparison of the Si (a) and nitrogen (b) depth profiles obtained by four different groups and from elastic recoil detection (ERD).

3. Discussion

The XPS profile reconstruction as presented is based on a number of simplifications, such as the uniqueness of the electron mean free path through the whole overlayer and neglecting elastic scattering. In addition, we identified a number of limitations in mathematical profile reconstruction. In order to verify the quantification uncertainty arising from these assumptions, a more physically based photoemission model was used (SESSA) to calculate spectra for multilayer systems. As mentioned earlier, its main limitation is the lack of an optimization procedure but, with a forward calculation, a more accurate answer is expected. While an XPS depth profile, as presented, typically slices the sample into 30 different layers of varying composition, the use of SESSA implies (for practical reasons) the limitation of the number of layers simulated with this procedure.

For the first system, a triple-layer model (C/HfO_2/SiO_2/Si) based on thicknesses as determined by ARXPS was used. An already good qualitative agreement was observed between the simulated intensities and the measured ones (not shown). However, significant differences were seen in the O and Hf intensities, where the calculated O intensities were smaller than the experimental ones and the calculated Hf intensities were larger than the experimental ones. As the reconstructed XPS profiles from the ARXPS data also show an increase in oxygen concentration toward the surface that can be explained by water adsorption on top of HfO_2, an additional oxygen layer was added in the model. Each layer thickness was adapted in order to achieve the best agreement between experimental and theoretical intensities. The comparison of the theoretical concentration profile as a function of angle determined by SESSA after optimization of the model system and the experimental concentration from ARXPS is presented in Fig. 11, showing that an excellent agreement between theory and experiment is possible. The final structure used for the theoretical simulation was the following: C/O/HfO_2/SiO_2/Si with a thickness of 2.3/1/22/10/Si Å, respectively. This structure remains very close to the structure determined from experimental data using the ARPROCESS software and shows that

Redistribution subject to AVS license or copyright; see http://scitation.aip.org/termsconditions. Download to IP: 130.54.110.72 On: Mon, 08 Sep 2014 03:00:35

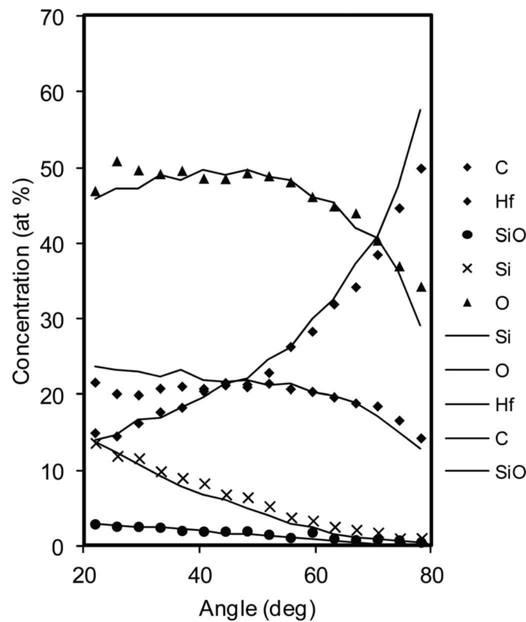

FIG. 11. Comparison of measured x-ray photoelectron spectroscopy (XPS) concentrations of sample 2 (group 1) (dots) and of the simulated concentrations calculated using Simulation of Electron Spectra for Surface Analysis (SESSA) (lines).

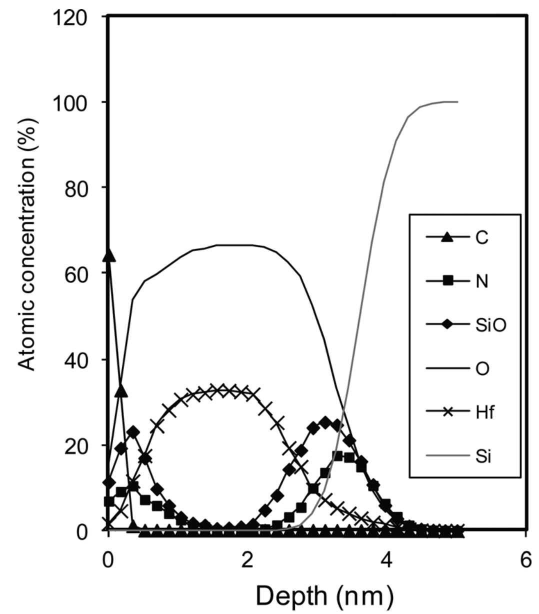

FIG. 12. Composition profile of an SiON/HfO_2/SiON/Si stack reconstructed with the angle-resolved x-ray photoelectron spectroscopy (ARXPS) profile reconstruction algorithm based on theoretical XPS intensities obtained by Simulation of Electron Spectra for Surface Analysis (SESSA).

even a simplified model allows one to obtain quantitative profiles from ARXPS.

Similarly, for the system comprising an SiON interfacial layer, the validity of the structure as determined by the simplified reconstruction can also be estimated. The structure determined with the multilayer model was 0.19 nm C/2.30 nm HfO_2/1.62 nm $SiO_{1.63}N_{0.18}$/Si, while the optimized structure obtained by SESSA was 0.21 nm C/0.1 nm O/2.07 nm HfO_2/1.38 nm $SiO_{1.43}N_{0.28}$. As for the HfO_2/SiO_2 system, a thinner HfO_2 layer had to be introduced. The thinner observed interfacial layer arises from a change in mean free path used in the calculation. Indeed, the modification of the mean free path due to the incorporation of nitrogen in the interfacial layer is not taken into account in the multilayer model thickness calculation but is present in the SESSA calculation. It is not clear why the difference is observed in the HfO_2 thickness.

In the reconstructed profiles from samples 4 and 5, we also observed a poor quality nitrogen profile at the surface, which deviates substantially from the process flow. In order to determine if this poor nitrogen profile at the surface is a consequence of the profile reconstruction algorithm itself or from the data quality, a further comparison with profile reconstruction using SESSA was made. For this purpose, a structure representing as close as possible the structure deduced from the ERD profile (Bulk Si/1.5 nm $SiO_{1.27}N_{0.49}$/2.2 nm HfO_2/0.54 nm $SiO_{1.27}N_{0.49}$/0.2 nm C) was used to simulate XPS intensities with SESSA. These intensities were used as input in the profile reconstruction algorithm in order to determine the resulting composition profile. It is observed that, in this case, the double nitrogen structure at the surface and the interface is nicely reproduced (Fig. 12). This indicates that the poor nitrogen profile at the surface is linked to the quality of the experimental data (including data treatment) rather than to the profile reconstruction methods. This is indeed not surprising as deconvoluting the nitrogen from the plasmon loss of the Hf peak is very difficult.

With the different models/analysis techniques, we may also quantitatively compare the amount of each element detected, which is presented in Fig. 13. Taking the ERD profile as reference, we observed that a good agreement (within 2%–3%) is obtained for the Hf coverage deduced from the full composition profile for all three techniques (XPS, ERD,

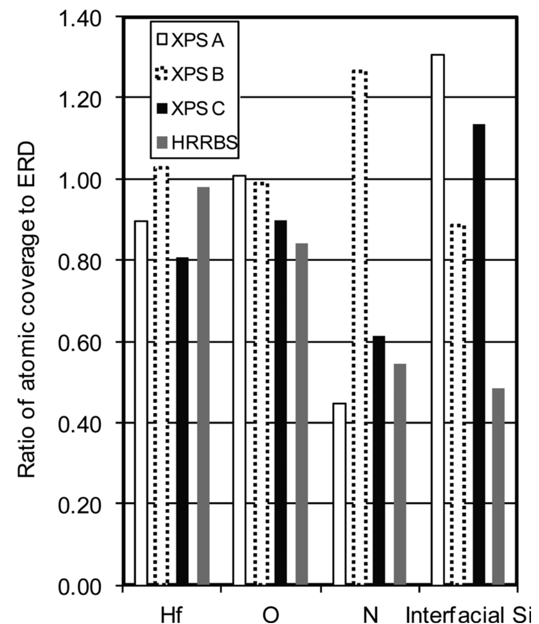

FIG. 13. Comparison for sample 3 of the Hf, O, and N coverage obtained using different models by x-ray photoelectron spectroscopy (XPS) and by high-resolution Rutherford backscattering spectrometry (HR-RBS). The coverage values are given relative to the coverage values measured by elastic recoil detection (ERD). The interfacial Si is calculated from the excess oxygen measured at the interface using the nuclear techniques.

Redistribution subject to AVS license or copyright; see http://scitation.aip.org/termsconditions. Download to IP: 130.54.110.72 On: Mon, 08 Sep 2014 03:00:35

HR-RBS). The Hf coverage estimated from the homogeneous layer model by XPS or from SESSA reconstruction is slightly underestimated (10%–20%). The total oxygen coverage is also in good agreement for the XPS layer model or XPS profile, but underestimated for the SESSA model or the HR-RBS. The underestimation of the SESSA concentration is a direct consequence of the necessary reduction of the HfO_2 layer thickness to match the theoretical concentration to the experimental ones. The lower oxygen coverage from HR-RBS may be linked to the lower sensitivity of RBS for light elements, as already observed for nitrogen.[35] Much larger errors are observed for the nitrogen coverage. The closest value is obtained by the XPS full profile reconstruction but still lies 20% from the ERD value. This larger intensity, linked to the apparent presence of nitrogen in the HfO_2 layer, is also an indication that some intensity attributed to nitrogen arises from the interfering Hf intensity. Other methods lead to 40%–60% errors. The underestimation of HR-RBS has been attributed to the lower sensitivity of the RBS to light elements; it is, however, not clear why the SESSA model of the XPS layer model leads to such an underestimation.

IV. SUMMARY AND CONCLUSION

This study shows that depth profiles reconstructed by ARXPS can be reliably used and similar results can be obtained at different sites. The accuracy of the reconstruction, however, depends upon a number of factors:

(1) The extraction of the individual peak intensities needs to be done accurately and in a systematic way. This implies that, in the case of interfering peaks, a correct separation of each element intensities should be possible. This is best done by using reference data rather than synthetic peaks.
(2) For thickness layer calculation a correct layer structure needs to be used. Uncertainties about the model can be resolved by using angle-resolved measurements and associated reconstructed depth profiles.
(3) To limit the uncertainties in the reconstruction the modeling should include chemical information (stoichiometry).
(4) Higher statistical noise increases the uncertainties of the measured intensities, which, in turn, lead to a depth profile quality degradation. This agrees with results published by Cumpson.[36]
(5) The physical parameters used in the depth profile reconstruction are critical to the quantification accuracy. The most important parameter is the mean free path. Using the attenuation length from the NIST database 82 provides a good agreement with profiles obtained by ERD.

[1] C. Adelmann, C. V. Sriramkumar, S. Van Elshocht, P. Lehnen, T. Conard, and S. Gendt, Appl. Phys. Lett. **91**, 162902 (2007).
[2] S. Van Elshocht, M. Caymax, S. De Gendt, T. Conard, J. Petry, L. Date, D. Pique, and M. M. Heyns, J. Electrochem. Soc. **151**, F77 (2004).
[3] G. Mavrou, K. Argyropoulos, A. Dimoulas, J. C. Hooker, T. Conard, and M. Butcher, Mater. Sci. Eng., B **109**, 85 (2004).
[4] J. S. Cable and J. C. S. Woo, IEEE Trans. Electron Devices **39**, 607 (1992).
[5] S. P. Tay and J. P. Ellul, J. Electron. Mater. **21**, 45 (1992).
[6] A. Halimaoui, E. Henrisey, and C. Hernandez, Mater. Res. Soc. Symp. Proc. **532**, 159 (1998).
[7] K. Kimura, K. Nakajima, T. Conard, W. Vandervorst, A. Bergmaier, and G. Dollinger, Nucl. Instrum. Methods Phys. Res. B **268**, 1960 (2010).
[8] M. A. Reading, J. A. van den Berg, P. C. Zalm, D. G. Armour, P. Bailey, T. C. Q. Noakes, A. Parisini, T. Conard, and S. De Gendt, J. Vac. Sci. Technol. B **28**, C1C65 (2010).
[9] G. Dollinger, C. M. Frey, A. Bergmaier, and T. Faestermann, Europhys. Lett. **42**, 25 (1998).
[10] B. Brijs *et al.*, Nucl. Instrum. Methods Phys. Res. B **161**, 429 (2000).
[11] K. Kimura, K. Nakajima, T. Conard, W. Vandervorst, A. Bergmaier, and G. Dollinger, Anal. Sci. **26**, SI 223 (2010)
[12] C. R. Brundle, G. Conti, and P. Mack, J. Electron Spectrosc. Relat. Phenom. **178**, 433 (2010).
[13] A. Herrera-Gomez *et al.*, Surf. Interface Anal. **41**, 840 (2009).
[14] M. A. Douglas, S. Hattangady, and K. Eason, J. Electrochem. Soc. **147**, 1893 (2000).
[15] J. G. M. van Berkum, M. J. P. Hopstaken, J. H. M. Snijders, Y. Tamminga, and F. Cubaynes, Appl. Surf. Sci. **203**, 414 (2003).
[16] H. De Witte, T. Conard, W. Vandervorst, and R. Gijbels, Appl. Surf. Sci. **203**, 523 (2003).
[17] T. Conard, W. Vandervorst, H. De Witte, and S. Van Elshocht, Appl. Surf. Sci. **231**, 581 (2004).
[18] W. Vandervorst, J. Bennett, C. Huyghebaert, T. Conard, C. Gondran, and H. De Witte, Appl. Surf. Sci. **231**, 569 (2004).
[19] J. Bennett, M. Beebe, C. Sparks, C. Gondran, and W. Vandervorst, Appl. Surf. Sci. **231**, 565 (2004).
[20] C. J. Powell, W. S. M. Werner, and W. Smekal, Appl. Phys. Lett. **89**, 172101 (2006).
[21] T. Conard, unpublished data for failed systems.
[22] L. Nyns *et al.*, J. Electrochem. Soc. **153**, F205 (2006).
[23] M. L. Green *et al.*, J. Appl. Phys. **92**, 7168 (2002).
[24] M. Meuris, P. W. Mertens, A. Opdebeeck, H. F. Schmidt, M. Depas, G. Vereecke, M. M. Heyns, and A. Philipossian, Solid State Technol. **38**, 109 (1995).
[25] H. H. Tseng *et al.*, IEEE Electron Device Lett. **23**, 704 (2002).
[26] S. Tanuma, C. J. Powell, and D. R. Penn, Surf. Interface Anal. **21**, 911 (1994).
[27] NIST Standard reference database 82; http://www.nist.gov/srd/nist82.cfm
[28] See: www.webelements.com
[29] R. Champaneria, P. Mack, R. White, and J. Wolstenholme, Surf. Interface Anal. **35**, 1028 (2003).
[30] J. P. Chang *et al.*, J. Appl. Phys. **87**, 4449 (2000).
[31] W. Smekal, W. S. M. Werner, and C. J. Powell, Surf. Interface Anal. **37**, 1059 (2000).
[32] See: http://www.nist.gov/srd/nist100.cfm
[33] G. Amsel and G. Battistig, Nucl. Instrum. Methods Phys. Res. B **240**, 1 (2005).
[34] A. Bergmaier, J. A. Van Den Berg, T. Conard, and W. Vandervorst, IBA 2007, Radebeul, Germany (unpublished).
[35] K. Kimura *et al.*, Surf. Interface Anal. **40**, 423 (2008).
[36] P. J. Cumpson, J. Electron Spectrosc. Relat. Phenom. **73**, 25 (1995).

Redistribution subject to AVS license or copyright; see http://scitation.aip.org/termsconditions. Download to IP: 130.54.110.72 On: Mon, 08 Sep 2014 03:00:35